FUNDAMENTALS & APPLICATIONS

CHEMELECTROCHEM

ANALYSIS & CATALYSIS, BIO & NANO, ENERGY & MORE

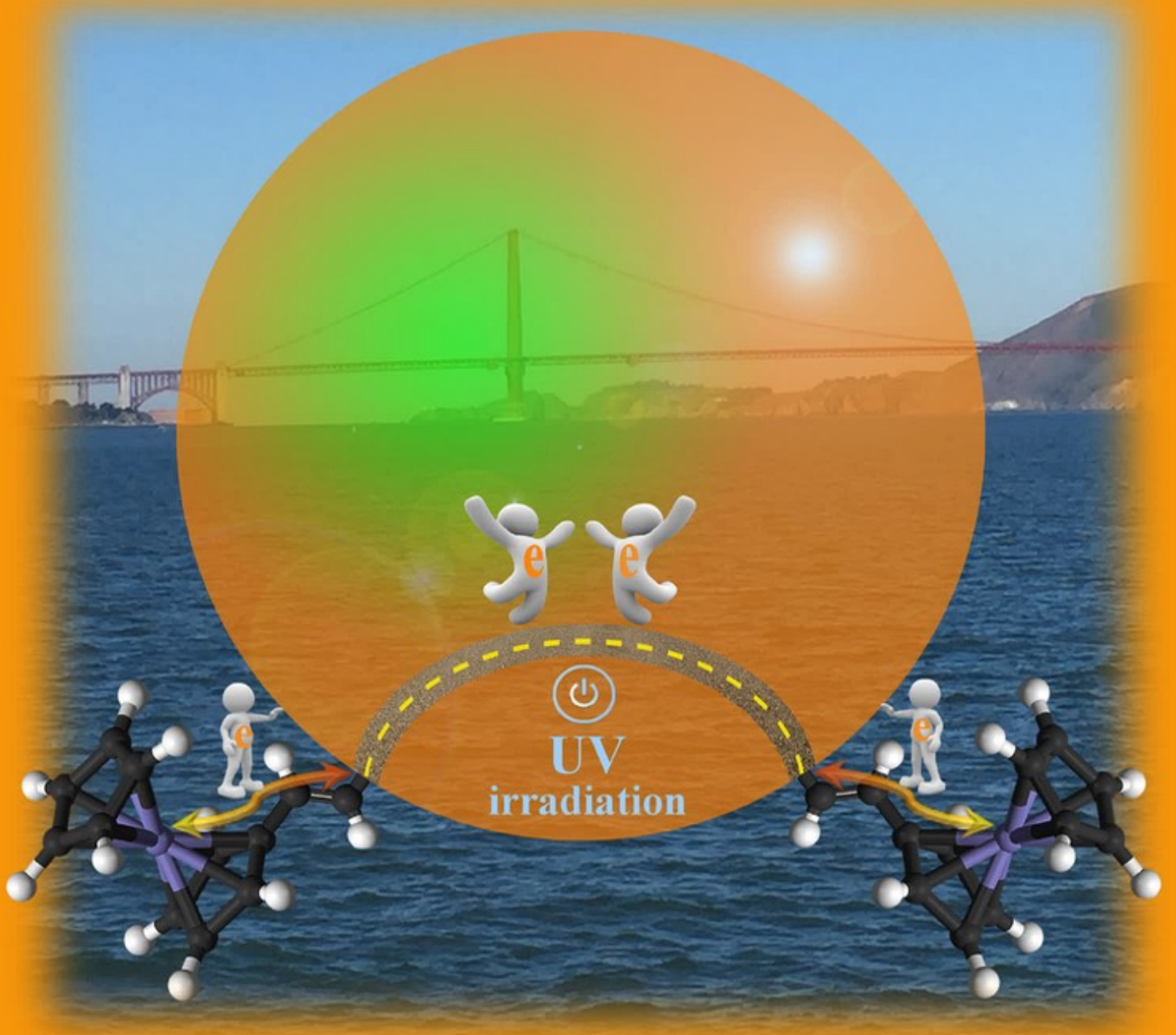

8/2016

Cover Picture:

S. Chen and co-workers

Intervalence Charge Transfer Mediated by Silicon Nanoparticles

A Journal of

ChemPubSoc Europe

WILEY-VCH

www.chemelectrochem.org

ChemPubSoc Europe
DOI: 10.1002/celc.201600114
CHEMELECTROCHEM Articles

Special Issue

Intervalence Charge Transfer Mediated by Silicon Nanoparticles

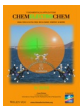

Yi Peng, Christopher P. Deming, and Shaowei Chen*[a]

Stable silicon nanoparticles (SiNPs) were synthesized by using a wet chemical method with (3-aminopropyl)triethoxysilane as the silicon source and ethynylferrocene as the capping ligands by taking advantage of the unique chemical reactivity of acetylene moieties with silicon hydride on the nanoparticle surface, forming Si–CH=CH– interfacial bonds under UV photoirradiation. Transmission electron microscopic measurements showed good dispersion of the nanoparticles with an average core diameter of 2.96 ± 0.46 nm. From UV/Vis absorption measurements, the nanoparticle bandgap was estimated to be 2.6 eV. XPS measurements confirmed the successful attachment of ethynylferrocene ligands onto the nanoparticle surface, with a footprint consistent with that of ferrocene. Electrochemically, the nanoparticles exhibited only one pair of voltammetric waves in the dark, suggesting a lack of effective electronic communication between the particle-bound ferrocenyl moieties, because of the low conductivity of the nanoparticle cores; whereas, under UV photoirradiation (365 nm), two pairs of voltammetric peaks were observed, with a potential spacing of 125 mV, suggesting that the nanoparticles behaved analogously to a Class II compound. This was ascribed to photo-enhanced electronic conductivity of the nanoparticle cores that facilitated intervalence charge transfer of the particle-bound ferrocene moieties.

1. Introduction

Intervalence charge transfer (IVCT) refers to a unique phenomenon observed with organometallic complexes consisting of multiple metal centers that are linked by conjugated chemical linkers, such as ferrocene oligomers and the Creutz–Taube ion. At mixed valence, rapid charge transfer occurs between the metal centers, leading to the emergence of new optical and electrochemical properties.[1] Recently, it has been found that IVCT may also be achieved with functional moieties bound onto (transition-metal) nanoparticle surfaces through conjugated metal–ligand interfacial bonds, where the metallic nanoparticle cores serve as the conducting media to facilitate intraparticle charge delocalization.[2] In fact, even a small variation in the valence state of the nanoparticle cores through chemical reduction (oxidation) has been shown to cause an apparent manipulation of the charge delocalization between nanoparticle-bound functional moieties.[3] In addition, by incorporating multiple functional groups on the nanoparticle surface, specific binding to selective ions/molecules has also been found to impact the electronic energy of the metal cores through electrostatic polarization and, therefore, intraparticle charge delocalization, as manifested in a deliberate variation of the nanoparticle optical/electronic characteristics. This unique feature may be exploited for the sensitive and selective detection of diverse chemical species.[4]

Indeed, experimentally, a variety of conjugated metal–ligand interfacial bonds have recently been formed for nanoparticle surface functionalization. For instance, metal–vinylidene (M=C=CH–) or metal–acetylide (M–C≡) bonds have been formed by taking advantage of the strong affinity of acetylene derivatives to transition-metal surfaces.[5] Such interfacial bonds may also be formed by using olefin derivatives as the capping ligands for platinum nanoparticles, owing to platinum-catalyzed dehydrogenation of the vinyl moieties to acetylene groups.[6] Upon the self-assembly of diazo derivatives on metal surfaces (with concurrent release of nitrogen), metal–carbene (M=C) π bonds may also be formed at the metal–ligand interface.[2] Additionally, metal–nitrene (M=N) π bonds have also been formed where nitrene radicals are produced through controlled thermolysis of azide derivatives.[7]

It has to be noted that these prior studies are primarily limited to transition-metal nanoparticles. An immediate question arises: Will effective intraparticle charge delocalization still occur when the functional moieties are bonded to semiconductor nanoparticles instead? Note, that with an apparent bandgap, the electronic conductivity of semiconductor nanoparticles will be markedly lower than that of the metal counterparts, which is anticipated to diminish intraparticle charge delocalization, as the nanoparticle cores behave equivalently to the chemical linkers bridging the functional moieties. Within this context, photoirradiation with photon energy greater than the nanoparticle bandgap will lead to enhanced nanoparticle electronic conductivity and, hence, nanoparticle-mediated electronic communication between the particle-bound functional moieties. This is the primary motivation of the present study.

[a] Y. Peng, C. P. Deming, Prof. Dr. S. Chen
Department of Chemistry and Biochemistry
University of California
1156 High Street, Santa Cruz, CA 95064 (USA)
E-mail: shaowei@ucsc.edu

Special Issue Invited contribution to a Special Issue on Monolayer-Protected Clusters

Herein, we used ethynylferrocene-functionalized silicon nanoparticles to examine IVCT mediated by semiconductor nanoparticles. The silicon nanoparticles were prepared by using a wet chemistry method with (3-aminopropyl)triethoxysilane (APTES) as the silicon source. HF etching led to the formation of hydrogenated silicon surfaces, which reacted readily with ethynylferrocene (EFc) forming Si–CH=CH–Fc interfacial bonds under UV irradiation. The resulting ferrocene-functionalized silicon nanoparticles (SiEFc) exhibited a bandgap of about 2.6 eV. In the dark, only one pair of voltammetric peaks were observed in electrochemical measurements of the nanoparticles in solution; whereas, under UV irradiation (365 nm, 3.40 eV), two pairs of voltammetric waves were observed instead, with a potential spacing consistent with IVCT of Class II compounds. Such photochemical activity was not observed when the nanoparticles were functionalized with vinylferrocene (VFc), forming Si–CH_2–CH_2–Fc saturated bonds at the nanoparticle–ligand interface.

2. Results and Discussion

The synthetic method is schematically illustrated in Scheme 1. Briefly, APTES is reduced by L-ascorbic acid whilst under vigorous stirring for 2 h, producing SiNPs, as based on a previous report with some modification.[8] HF treatment led to the effective removal of a thin oxide layer on the nanoparticle surface, forming hydrogenated silicon nanoparticles (SiHNPs).[10] The surface Si–H moieties are known to exhibit unique chemical reactivity, undergoing hydrosilylation reactions with acetylene (HC≡C–R) and olefin (CH_2=CH–R) derivatives under UV photoirradiation, forming Si–CH=CH–R and Si–CH_2–CH_2–R bonds, respectively.[9] This was exploited for the functionalization of the SiNPs with ethynylferrocene and vinylferrocene, producing SiEFc and SiVFc with the formation of Si–CH=CH–Fc and Si–CH_2–CH_2–Fc interfacial bonds, respectively.

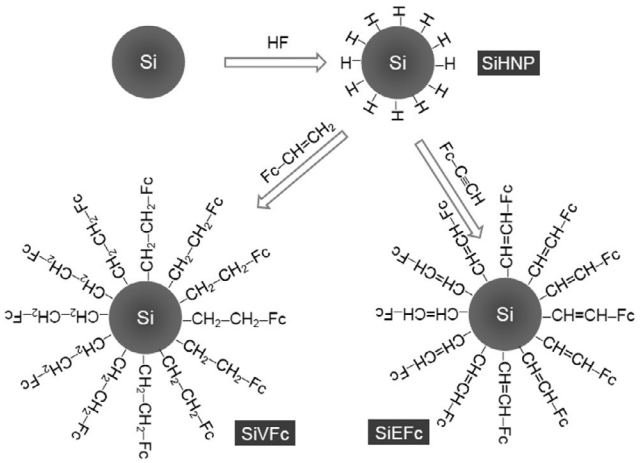

Scheme 1. Schematic diagram of the synthesis of SiEFc and SiVFc nanoparticles.

The structure of the resulting nanoparticles was first characterized by using TEM measurements. Figure 1 A depicts a representative TEM image of the SiEFc nanoparticles. One can see that the nanoparticles were rather uniform in size and well dispersed without apparent agglomeration, suggesting sufficient protection of the nanoparticles by the organic capping ligands. Statistical analysis based on more than 150 nanoparticles showed that the average core diameter of the nanoparticles was estimated to be 2.96 ± 0.46 nm, as manifested in the core-size histogram in the inset of Figure 1 A. In addition, well-defined lattice fringes can readily be identified in high-resolution TEM measurements, even without any post-synthesis annealing, where the lattice spacing of 0.30 nm is consistent with the interplanar distance of Si(111) crystalline planes (JCPDS card No. 00-001-0787), as depicted in Figure 1 B. Consistent results were obtained with the SiVFc nanoparticles.

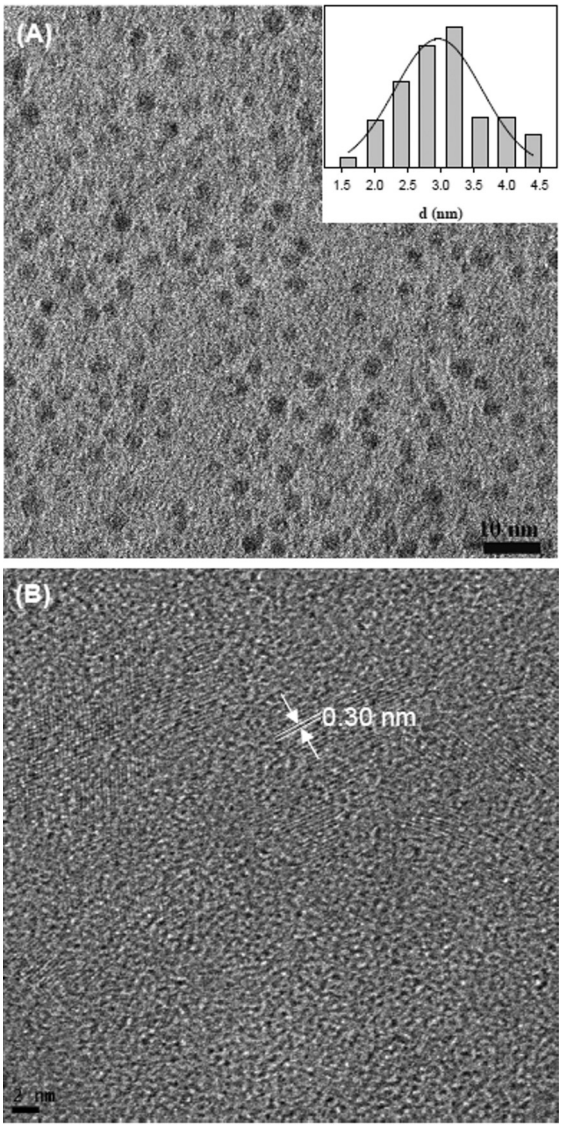

Figure 1. Representative TEM images of SiEFc nanoparticles. Scale bars are A) 10 nm and B) 2 nm. Inset is the core-size histogram.

As the Bohr radius of bulk silicon is about 4.3 nm,[11] the fact that the resulting nanoparticles are markedly smaller suggests strong quantum confinement effect.[12] Note that the bandgap (E_g^{NP}) of semiconductor nanoparticles may be estimated by the

following equation, $E_g^{NP} = E_g^{bulk} + \frac{h^2}{8r^2}\left(\frac{1}{m_h} + \frac{1}{m_e}\right)$, where E_g^{bulk} is the bulk bandgap, h is Planck's constant, r is the nanoparticle core radius, m_h and m_e are the effective mass of the hole and electron, respectively.[13] For the SiEFc nanoparticles synthesized above, $m_h = 0.286\ m_o$ and $m_e = 0.19\ m_o$ with m_o being the electron rest mass, and thus E_g^{NP} was estimated to be approximately 2.63 eV, in comparison to 1.12 eV for bulk Si.[11,14] This is in good agreement with results obtained from nanoparticle UV/Vis absorption measurements. Note, that prior research has shown that silicon nanoparticles exhibit mostly an indirect bandgap;[14] thus, when $(\alpha h\nu)^{1/2}$ is plotted against $(h\nu - E_g)$, with α being the optical absorbance and $h\nu$ the photon energy, extrapolation of the spectrum to the x axis (dashed line, Figure 2) may be exploited for the quantitative assessment of the nanoparticle bandgap, which was approximately 2.59 eV. Consistent results were obtained in photoluminescence measurements. As depicted in the inset to Figure 2, one can see that the SiEFc nanoparticles exhibited a clearly defined excitation peak at 412 nm (3.01 eV) along with an emission peak at 496 nm (2.50 eV), where the asymmetry of the photoluminescence profiles might be partly ascribed to stronger oscillator strength of smaller nanoparticles.[14] Similar behaviors were observed with SiVFc nanoparticles.

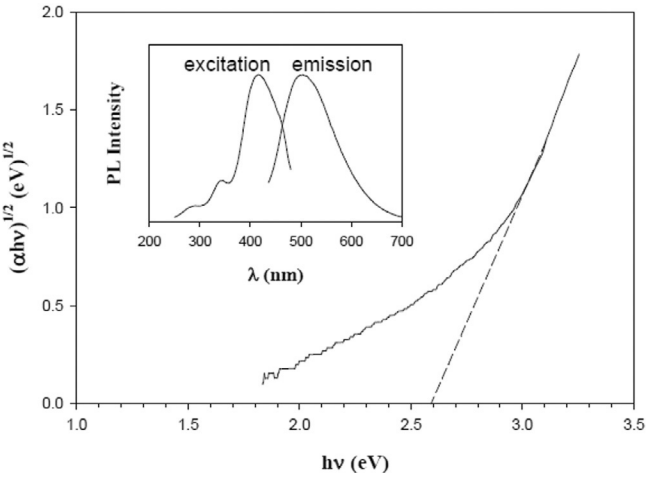

Figure 2. UV/Vis spectrum of SiEFc nanoparticles in toluene; α is the absorbance and $h\nu$ is the photon energy. Dashed line is the linear extrapolation to the x axis. Inset: excitation and emission spectra of the same nanoparticle solution.

The successful binding of the EFc ligands onto the nanoparticle surface was confirmed by using FTIR measurements. From Figure 3, one can see that monomeric EFc exhibits several characteristic vibrational features, including the terminal ≡C–H stretch at 3294 cm^{-1}, C≡C stretch at 2105 cm^{-1}, ferrocenyl skeleton vibrations (C=C) at 1400–1500 cm^{-1}, and ring =C–H stretch at 3094 cm^{-1}.[15] Yet, upon hydrosilylation reactions with Si–H on the silicon nanoparticles, both the ≡C–H and C≡C vibrational stretches vanished, whereas the ferrocenyl C=C and ring =C–H stretches remained, which is consistent with the binding of EFc ligands onto the nanoparticle surface forming Si–CH=CH–Fc interfacial linkages, as depicted in Scheme 1 (the corresponding C=C vibration can be found at 1655 cm^{-1}).[16] This also indicates that the resulting SiEFc nanoparticles were free of excess EFc monomers. The fact that no vibrational feature was observed at approximately 2100 cm^{-1} indicates the very efficient reaction of the surface Si–H groups with the EFc ligands. Similar spectral characteristics can be seen with the SiVFc nanoparticles, except that no interfacial C=C vibration was observed at 1655 cm^{-1}.

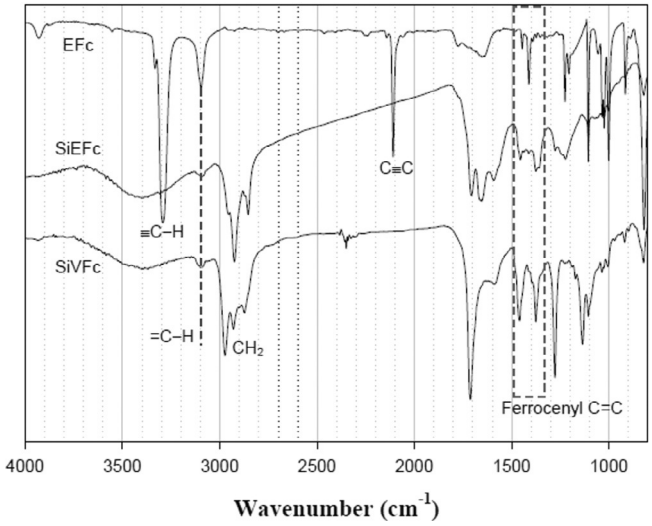

Figure 3. FTIR spectra of EFc monomers, SiEFc and SiVFc nanoparticles.

Further structural characterizations were then carried out by using XPS measurements. From the survey spectrum in Figure 4A, the Si 2p, C 1s, and Fe 2p electrons can be readily identified at approximately 100, 285, and 720 eV, respectively (along with O 1s electrons at ca. 532 eV). Panel B depicts the high-resolution scan of the Si 2p electrons, where deconvolution yields two sub-peaks at 98.8 and 101.6 eV. The former

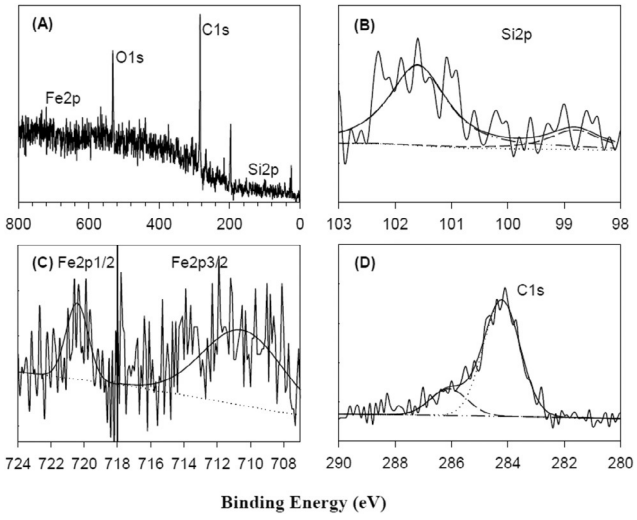

Figure 4. A) XPS survey spectrum of SiEFc nanoparticles, and high-resolution scans of the corresponding B) Si 2p, C) Fe 2p, and D) C 1s electrons. Spiky curves are experimental data and smooth curves are deconvolution fits.

may be assigned to elemental Si of the nanoparticle cores, whereas the latter likely entails the combined contributions of Si in the Si–CH=CH–Fc interfacial linkages as well as residual APTES ligands, but not SiO_2, which is markedly higher at approximately 103 eV.[17] For the Fe 2p electrons in panel C, two peaks can be resolved at 710.6 eV (Fe $2p_{3/2}$) and 720.4 eV (Fe $2p_{1/2}$), consistent with those of ferrocene derivatives.[18] The C 1s spectrum is shown in panel D, where a major peak can be observed at 284.2 eV, likely arising from ferrocenyl carbons,[19] whereas the minor peak at 286.1 eV is consistent with carbon in C–O bonds from residual APTES ligands. Taken together, these results confirmed the surface functionalization of the silicon nanoparticles by the EFC ligands forming Si–CH=CH–Fc interfacial bonds (Scheme 1). Furthermore, based on the integrated peak areas of the Fe 2p and Si 2p electrons, the atomic ratio of Fe/Si was estimated to be 0.088:1. Given that the nanoparticle core diameter is 2.96 nm (Figure 1) and the density of bulk silicon is 2.328 g cm^{-3}, one can therefore estimate the footprint of one EFc ligand on the nanoparticle surface to be 0.46 nm^2, which is in excellent agreement with the cross-sectional area of the ferrocenyl moiety (0.45 nm^2).[20] This suggests an almost full monolayer of EFc ligands on the nanoparticles, consistent with the good dispersion of the nanoparticles observed in TEM measurements (Figure 1).

The electron-transfer properties of the SiEFc nanoparticles were then examined by voltammetric measurements. Figure 5 A depicts the square-wave voltammograms (SWVs) of the SiEFc nanoparticles at a concentration of 10 mg mL^{-1} in DMF with 0.1 M TBAP as the supporting electrolyte (SWV was employed primarily to enhance peak resolution). When the voltammograms were acquired in the dark (dotted curves), a single pair of voltammetric peaks can be seen clearly standing out of the featureless background (dashed curves) within the potential range of −0.2 to +0.3 V, with the formal potential $E^{\circ\prime} = +0.084$ V (vs. Fc^+/Fc), which is attributable to the redox reaction of the ferrocene moieties bound on the silicon nanoparticle surface, $Fc^+ + e^- = Fc$. One may notice that despite the formation of Si–CH=CH–Fc bonds at the nanoparticle–ligand interface, no apparent IVCT was observed with SiEFc nanoparticles, which might be ascribed to the low electrical conductivity of the Si cores that limited intraparticle charge transfer because of the substantial bandgap (Figure 2). This is in contrast with earlier results obtained with metal nanoparticle cores.[2] Interestingly, upon exposure to UV photoirradiation (365 nm or 3.40 eV, 6 W), the voltammetric peaks became asymmetrically broadened, and deconvolution actually yielded two pairs of peaks with the formal potentials at −0.032 and +0.093 V, respectively (medium and long dashed curves). The appearance of two pairs of voltammetric peaks, instead of one, strongly suggests that IVCT occurred between the nanoparticle-bound ferrocenyl moieties. This is likely facilitated by the photo-enhanced electrical conductivity of the nanoparticle cores.[21]

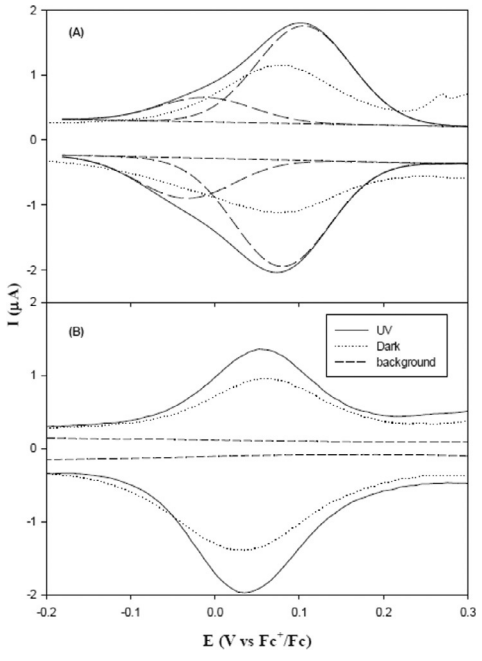

Figure 5. SWVs of A) SiEFc and B) SiVFc nanoparticles in 0.1 M TBAP in DMF in the dark and under UV photoirradiation (365 nm, 6 mW). SWVs collected with the blank supporting electrolyte are also included. Nanoparticle concentration: 10 mg mL^{-1}; increment of potential: 2 mV; amplitude: 25 mV; frequency: 15 Hz. Long and medium dashed curves in (A) are the deconvolution fits of the voltammograms acquired under UV photoirradiation.

As mentioned earlier, nanoparticle-mediated IVCT has been observed mainly with metal nanoparticles. For instance, when ferrocene moieties were bound onto ruthenium nanoparticle surfaces by ruthenium–carbene π bonds (Ru=CH-Fc), two pairs of voltammetric waves were observed with a peak spacing of about 200 mV,[2] consistent with Class II compounds as defined by Robin et al. and Day et al.[1b,g] In the present study, the peak spacing of 125 mV is smaller, indicating diminished electronic communication through the semiconducting particle cores, although it remains within the range of Class II classification. Nevertheless, it should be noted that, in the earlier study with ferrocene-functionalized carbon nanoparticles, the peak spacing was only 107 mV under UV photoirradiation, which was 40 mV greater than that observed in the dark, and the nanoparticles were classified as a Class I/II compound.[18b] This is probably because of the lack of crystallinity of the carbon nanoparticles, leading to limited enhancement of the nanoparticle electrical conductivity of effects by photoirradiation.

In a prior study based on DFT calculations,[22] we examined the impacts of the length of the chemical bridge on IVCT of biferrocene derivatives and found that the Fc–$(CH{=}CH)_n$–Fc^+ mixed-valence compounds belonged to Class II, even at $n = 3$, in contrast to Fc–$(CH_2\text{-}CH_2)_n$–Fc^+, where the saturated spacers rendered the compound to behave as a Class I complex. This is in good agreement with the results observed above, with the SiEFc nanoparticles under UV photoirradiation. In fact, in the present study, when vinylferrocene was used instead for SiHNP surface functionalization, the resulting SiVFc nanoparticles were capped by saturated interfacial linkages of Si–CH_2–CH_2–Fc (Scheme 1). Electrochemical measurements exhibited only one pair of voltammetric waves ($E^{\circ\prime} = +0.054$ V) both in the dark and under UV photoirradiation, as manifested in Figure 5 B. This indicates that both the silicon nanoparticle cores

and the hydrocarbon spacers play a critical role in controlling the electronic communication between the particle-bound functional moieties.

3. Conclusions

In this study, silicon nanoparticles were synthesized through the chemical reduction of APTES. As the size of the nanoparticles was markedly smaller than the silicon Bohr radius, a marked quantum confinement effect was observed, as manifested by UV/Vis spectroscopic measurements, where the bandgap was estimated to be about 1.5 eV larger than that of bulk silicon. HF etching led to the formation of Si–H on the nanoparticle surface, which underwent photo-initiated hydrosilylation reactions with ethynylferrocene and vinylferrocene, forming Si–CH=CH–Fc and Si–CH_2–CH_2–Fc interfacial linkages, respectively. XPS measurements confirmed the formation of a compact monolayer of ligands on the nanoparticle surface. Interestingly, for the ethynylferrocene-functionalized nanoparticles, effective IVCT was observed in electrochemical measurements under UV photoirradiation, as manifested by the emergence of two pairs of voltammetric waves with a peak spacing of 125 mV, consistent with Class II compounds, in contrast to only one pair of peaks when the measurements were conducted in the dark. This was ascribed to photo-enhanced electrical conductivity of the nanoparticle cores that facilitated intraparticle charge delocalization of the nanoparticle-bound ferrocenyl groups. Control experiment with vinylferrocene-functionalized nanoparticles exhibited only a single pair of voltammetric peaks both in the dark and under similar UV photoirradiation, primarily because of the saturated interfacial linkage that impeded intraparticle charge transfer.

Experimental Section

Chemicals

(3-Aminopropyl)triethoxysilane (APTES, 99%, Acros), L-ascorbic acid (ACS grade, Amresco), sodium hydroxide (NaOH, extra pure, Acros), hydrofluoric acid (HF, 49%, Fisher scientific), vinylferrocene (VFc, 97%, Sigma–Aldrich), ethynylferrocene (EFc, 99%, Acros), calcium chloride ($CaCl_2$·6H2O), and tetrabutylammonium perchlorate (TBAP, 99%, Acros) were used as received. All solvents were obtained from typical commercial sources at their highest purity and used without further treatment. Water was supplied by a Barnstead Nanopure water system (18.3 MΩ cm).

Synthesis and Surface Functionalization of Silicon Nanoparticles

Ethynylferrocene-functionalized silicon (SiEFc) nanoparticles were synthesized by adopting a procedure reported in the literature.[8] In brief, APTES (5 mL) was added to N_2-saturated Nanopure water (20 mL) with magnetic stirring for 10 min, into which a 1:1 (v/v) mixture of 0.2 M L-ascorbic acid and 0.25 M NaOH (6.5 mL) was added. The resulting solution was subjected to magnetic stirring for another 2 h, where the emergence of an orange–red color signified the formation of silicon nanoparticles (SiNPs). The nanoparticle solution was then dried by rotary evaporation and the obtained solids were re-dissolved in 10 mL of a 1:1:1 (v/v/v) mixture of Nanopure water, ethanol, and hydrofluoric acid to form hydrogenated silicon nanoparticles (SiHNPs). Into this solution, EFc (30 mg) was added and then stirred vigorously overnight under UV photoirradiation (254 nm, 6 W).[9] $CaCl_2$ was subsequently added to precipitate excess hydrofluoric acid, and the solution part was collected and dried by rotary evaporation after the addition of methanol (40 mL). After centrifugation at 6000 rpm for 10 min, the supernatant was collected and condensed to 5 mL. Then, a large excess of hexane was added to remove remaining monomeric ethynylferrocence and the extraction was repeated five times, affording purified ethynylferrocene-functionalized silicon nanoparticles (SiEFc) in the methanol layer with the formation of Si–CH=CH–Fc interfacial bonds.

Vinylferrocene-functionalized silicon nanoparticles (SiVFc) were prepared in a similar fashion, except that VFc was used instead of EFc, where Si–CH_2–CH_2–Fc interfacial bonds were formed.

Characterization

The nanoparticle size and morphological features were characterized with transmission electron microscopy (TEM, Philips CM300 at 300 kV). X-ray photoelectron spectroscopic measurements were carried out with a PHI 5400/XPS instrument equipped with an Al K_α source operated at 350 W and at 10^{-9} Torr. UV/Vis spectroscopic studies were carried out with an ATI Uni-cam UV4 spectrometer. FTIR measurements were carried out with a PerkinElmer FTIR spectrometer (Spectrum One), where the samples were prepared by compressing the samples into a KBr pellet. The spectral resolution was 4 cm^{-1}.

Electrochemistry

Voltammetric measurements were performed with a CHI 440 electrochemical workstation. A polycrystalline gold disk electrode (sealed in glass tubing) was used as the working electrode. A Pt coil and a Ag/AgCl wire were used as counter electrode and reference electrode, respectively. The gold electrode was first polished with alumina slurries (0.05 μm) and then cleaned with sonication in H_2SO_4 and Nanopure water. Prior to data acquisition, the electrolyte solution was deaerated by bubbling ultrahigh-purity N_2 for at least 20 min and blanketed with a nitrogen atmosphere during the entire experimental procedure. Voltammograms were acquired both in the dark and under UV photoirradiation with a UV light source (365 nm, 6 W). Note, that the potentials were calibrated against the formal potential of ferrocene monomers (Fc^+/Fc) in the same electrolyte solution.

Acknowledgements

This work was supported in part by the National Science Foundation (CHE-1265635 and DMR-1409396). TEM and XPS work was carried out at the National Center for Electron Microscopy and Molecular Foundry at the Lawrence Berkeley National Laboratory as part of a user project.

Keywords: ferrocene · hydrosilylation · interfacial bond · intervalence charge transfer · silicon nanoparticle

[1] a) D. O. Cowan, C. Levanda, J. Park, F. Kaufman, *Acc. Chem. Res.* **1973**, *6*, 1–7; b) P. Day, N. S. Hush, R. J. H. Clark, *Philos. Trans. R. Soc. London Ser. A* **2008**, *366*, 5–14; c) D. R. Gamelin, E. L. Bominaar, C. Mathoniere, M. L. Kirk, K. Wieghardt, J. J. Girerd, E. I. Solomon, *Inorg. Chem.* **1996**, *35*, 4323–4335; d) R. D. Williams, V. I. Petrov, H. P. Lu, J. T. Hupp, *J. Phys. Chem. A* **1997**, *101*, 8070–8076; e) B. S. Brunschwig, C. Creutz, N. Sutin, *Chem. Soc. Rev.* **2002**, *31*, 168–184; f) H. Sun, J. Steeb, A. E. Kaifer, *J. Am. Chem. Soc.* **2006**, *128*, 2820–2821; g) M. B. Robin, P. Day, *Adv. Inorg. Chem. Radiochem.* **1968**, *10*, 247–422; h) O. S. Wenger, *Chem. Soc. Rev.* **2012**, *41*, 3772–3779.

[2] W. Chen, S. W. Chen, F. Z. Ding, H. B. Wang, L. E. Brown, J. P. Konopelski, *J. Am. Chem. Soc.* **2008**, *130*, 12156–12162.

[3] X. W. Kang, N. B. Zuckerman, J. P. Konopelski, S. W. Chen, *Angew. Chem. Int. Ed.* **2010**, *49*, 9496–9499; *Angew. Chem.* **2010**, *122*, 9686–9689.

[4] a) W. Chen, N. B. Zuckerman, J. P. Konopelski, S. W. Chen, *Anal. Chem.* **2010**, *82*, 461–465; b) X. W. Kang, X. Li, W. M. Hewitt, N. B. Zuckerman, J. P. Konopelski, S. W. Chen, *Anal. Chem.* **2012**, *84*, 2025–2030; c) P. G. Hu, Y. Song, M. D. Rojas-Andrade, S. W. Chen, *Langmuir* **2014**, *30*, 5224–5229; d) C. P. Deming, X. W. Kang, K. Liu, S. W. Chen, *Sens. Actuators B* **2014**, *194*, 319–324.

[5] a) W. Chen, N. B. Zuckerman, X. W. Kang, D. Ghosh, J. P. Konopelski, S. W. Chen, *J. Phys. Chem. C* **2010**, *114*, 18146–18152; b) X. W. Kang, N. B. Zuckerman, J. P. Konopelski, S. W. Chen, *J. Am. Chem. Soc.* **2012**, *134*, 1412–1415.

[6] P. G. Hu, P. N. Duchesne, Y. Song, P. Zhang, S. W. Chen, *Langmuir* **2015**, *31*, 522–528.

[7] X. W. Kang, Y. Song, S. W. Chen, *J. Mater. Chem.* **2012**, *22*, 19250–19257.

[8] Y. L. Zhong, F. Peng, F. Bao, S. Y. Wang, X. Y. Ji, L. Yang, Y. Y. Su, S. T. Lee, Y. He, *J. Am. Chem. Soc.* **2013**, *135*, 8350–8356.

[9] a) F. J. Hua, M. T. Swihart, E. Ruckenstein, *Langmuir* **2005**, *21*, 6054–6062; b) B. Fabre, *Acc. Chem. Res.* **2010**, *43*, 1509–1518; c) X. Y. Cheng, S. B. Lowe, P. J. Reece, J. J. Gooding, *Chem. Soc. Rev.* **2014**, *43*, 2680–2700.

[10] C. C. Shih, P. C. Chen, G. L. Lin, C. W. Wang, H. T. Chang, *ACS Nano* **2015**, *9*, 312–319.

[11] A. D. Yoffe, *Adv. Phys.* **2002**, *51*, 799–890.

[12] B. Delley, E. F. Steigmeier, *Appl. Phys. Lett.* **1995**, *67*, 2370–2372.

[13] M. A. Green, *J. Appl. Phys.* **1990**, *67*, 2944–2954.

[14] C. Meier, A. Gondorf, S. Luttjohann, A. Lorke, H. Wiggers, *J. Appl. Phys.* **2007**, *101*, 103112.

[15] a) Y. K. Gun'ko, T. S. Perova, S. Balakrishnan, A. A. Potapova, R. A. Moore, E. V. Astrova, *Phys. Status Solidi A* **2003**, *197*, 492–496; b) L. H. Guan, Z. J. Shi, M. X. Li, Z. N. Gu, *Carbon* **2005**, *43*, 2780–2785.

[16] R. M. Silverstein, G. C. Bassler, T. C. Morrill, *Spectrometric identification of organic compounds, 5th ed.*, John Wiley & Sons, Inc, New York, NY, **1991**.

[17] J. J. Romero, M. J. Llansola-Portoles, M. L. Dell'Arciprete, H. B. Rodriguez, A. L. Moore, M. C. Gonzalez, *Chem. Mater.* **2013**, *25*, 3488–3498.

[18] a) C. D. Wagner, W. M. Riggs, L. E. Davis, J. F. Moulder, G. E. Muilenberg, *Handbook of x-ray photoelectron spectroscopy : a reference book of standard data for use in x-ray photoelectron spectroscopy*, PerkinElmer Corp., Eden Prairie, Minn., **1979**; b) Y. Song, X. W. Kang, N. B. Zuckerman, B. Phebus, J. P. Konopelski, S. W. Chen, *Nanoscale* **2011**, *3*, 1984–1989.

[19] L. P. Méndes De Leo, E. de La Llave, D. Scherlis, F. J. Williams, *J. Chem. Phys.* **2013**, *138*, 114707.

[20] S. Campidelli, L. Perez, J. Rodriguez-Lopez, J. Barbera, F. Langa, R. Deschenaux, *Tetrahedron* **2006**, *62*, 2115–2122.

[21] S. Pradhan, S. W. Chen, J. Zou, S. M. Kauzlarich, *J. Phys. Chem. C* **2008**, *112*, 13292–13298.

[22] F. Z. Ding, H. B. Wang, Q. Wu, T. Van Voorhis, S. W. Chen, J. P. Konopelski, *J. Phys. Chem. A* **2010**, *114*, 6039–6046.

Manuscript received: February 28, 2016
Final Article published: March 10, 2016